Composite Structures 94 (2012) 3654–3663

Contents lists available at SciVerse ScienceDirect

Composite Structures

journal homepage: www.elsevier.com/locate/compstruct

Exact 3D stress analysis of laminated composite plates by sampling surfaces method

G.M. Kulikov *, S.V. Plotnikova

Department of Applied Mathematics and Mechanics, Tambov State Technical University, Sovetskaya Street, 106, Tambov 392000, Russia

ARTICLE INFO

Article history:
Available online 15 June 2012

Keywords:
Laminated plate
3D stress analysis
Layer-wise description
Angle-ply composite
Sampling surfaces method

ABSTRACT

A paper focuses on the use of the efficient approach to exact 3D elasticity solutions of cross-ply and angle-ply laminated composite plates. This approach is based on the new method of sampling surfaces (SaS) developed recently by the authors. We introduce inside the nth layer I_n not equally spaced SaS parallel to the midsurface of the plate and choose displacements of these surfaces as fundamental plate unknowns. Such an idea permits the representation of the proposed higher order layer-wise plate theory in a very compact form. This fact gives in turn the opportunity to derive the exact 3D solutions of elasticity for thick and thin laminated composite plates with a prescribed accuracy by utilizing a sufficiently large number of SaS, which are located at interfaces and Chebyshev polynomial nodes.

1. Introduction

Currently, the use of the layer-wise theory for the analysis of thick laminated composite plates is widely accepted. The most general form of layer-wise kinematics presented in Carrera's unified formulation [1] is written as

$$u_i^{(n)} = F_0 u_i^{[n-1]} + F_1 u_i^{[n]} + \sum_r F_r u_{ir}^{(n)}, \quad x_3^{[n-1]} \leqslant x_3 \leqslant x_3^{[n]},$$
$$F_0(x_3) = \frac{x_3^{[n]} - x_3}{h_n}, \quad F_1(x_3) = \frac{x_3 - x_3^{[n-1]}}{h_n}, \quad F_r\left(x_3^{[n-1]}\right) = F_r\left(x_3^{[n]}\right) = 0, \tag{1}$$

where $u_i^{(n)}(x_1, x_2, x_3)$ are the displacements of the nth layer ($i = 1,2,3$); $u_i^{[n-1]}(x_1, x_2)$ and $u_i^{[n]}(x_1, x_2)$ are the displacements of the bottom and top surfaces of the nth layer (interfaces); $u_{ir}^{(n)}(x_1, x_2)$ are the modal displacements of the nth layer ($r = 2,3,\ldots,R$); $F_r(x_3)$ are the prescribed polynomials of degree r; $x_3^{[n-1]}$ and $x_3^{[n]}$ are the transverse coordinates of layer interfaces $\Omega^{[n-1]}$ and $\Omega^{[n]}$ (Fig. 1); $h_n = x_3^{[n]} - x_3^{[n-1]}$ is the thickness of the nth layer; x_1 and x_2 are the Cartesian coordinates of the midsurface Ω; x_3 is the thickness coordinate normal to the midsurface; the index n identifies the belonging of any quantity to the nth layer and runs from 1 to N, where N is the number of layers. Historically, the first order layer-wise models [2–8] were first. A bit later, the second order models with $R = 2$ and third order models with $R = 3$ were developed [9–12]. The fourth order layer-wise model ($R = 4$) is utilized in Carrera's unified formulation [1], where polynomials F_r are evaluated as a difference between two Legendre polynomials of degrees r and $r - 2$. For a complete review, the reader is referred to survey articles [9,13–18].

In the present paper, we consider a new efficient method of SaS proposed recently by the authors [19–21]. As SaS denoted by $\Omega^{(n)1}, \Omega^{(n)2}, \ldots, \Omega^{(n)I_n}$, we choose outer surfaces and any inner surfaces inside the nth layer and introduce displacement vectors $\mathbf{u}^{(n)1}, \mathbf{u}^{(n)2}, \ldots, \mathbf{u}^{(n)I_n}$ of these surfaces as fundamental plate unknowns, where I_n is the total number of SaS chosen for each layer ($I_n \geqslant 3$). Such choice of displacements with the consequent use of Lagrange polynomials of degree $I_n - 1$ in the thickness direction for each layer permits the representation of governing equations of the laminated plate theory in a very compact form. An idea of this approach can be traced back to [22,23], where the equivalent single-layer theories with three [22], four and five [23] equally spaced SaS inside the shell body are considered. Herein, a general case with I_n not equally spaced SaS inside the nth layer is studied. Note also that the term SaS should not be confused with such terms as fictitious interfaces or virtual interfaces, which are extensively used in layer-wise theories. The main difference consists in the lack of possibility to employ the polynomials F_r of high degree in Eq. (1) because in conventional layer-wise descriptions only the third and fourth order through-the-thickness polynomial interpolations are admissible (see e.g. [1,17]). This restricts the use of the fictitious/virtual interfaces technique for derivation of the exact 3D elasticity solutions. On the contrary, the SaS method permits the use of polynomials of high degree. This fact gives in turn the opportunity to derive the exact 3D solutions for laminated composite plates with a prescribed accuracy utilizing a sufficiently large number of not equally spaced SaS.

It is important to mention that the developed approach with *equally spaced* SaS [19–21] does not work properly with Lagrange polynomials of high degree because the Runge's phenomenon [24] can occur, which yields the wild oscillation at the edges of the interval when the user deals with any specific functions. If the number of equally spaced nodes is increased then the oscillations

* Corresponding author.
E-mail address: gmkulikov@mail.ru (G.M. Kulikov).

0263-8223/$ - see front matter © 2012 Elsevier Ltd. All rights reserved.
http://dx.doi.org/10.1016/j.compstruct.2012.06.006

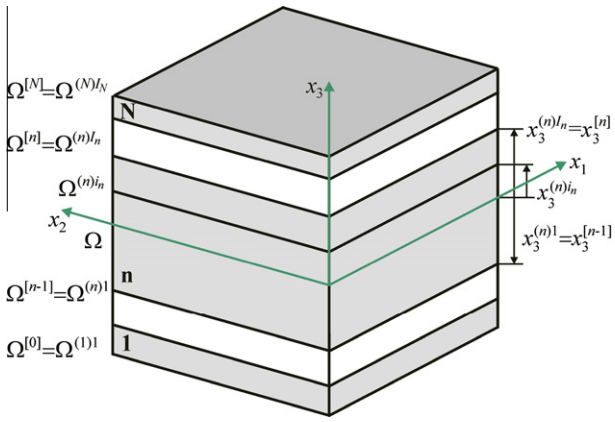

Fig. 1. Geometry of the thick laminated plate.

become even larger. Fortunately, the use of Chebyshev polynomial nodes [25] can help to improve significantly the behaviour of Lagrange polynomials of high degree for which the error will go to zero as $I_n \to \infty$.

The exact 3D solution of elasticity for simply supported isotropic plate was presented by Vlasov [26]. The extensions of Vlasov's solution to cross-ply laminated composite plates were done by Pagano [27], Srinivas and Rao [28,29] and Pagano and Hatfield [30]. Pagano presented the exact solution for the cylindrical bending of composite plates with general layups [31]. The developments for antisymmetric angle-ply laminates in the framework of 3D elasticity were carried out by Noor and Burton [32] and Savoia and Reddy [33]. The present paper is intended to show that the SaS method can be applied efficiently to the solution of aforementioned problems. It is necessary to note that the authors restrict themselves to finding *five right digits* in all examples presented. The better accuracy is possible of course but requires more SaS inside each layer to be taken.

2. Three dimensional description of laminated plate

Consider a thick laminated plate of the thickness h. The transverse coordinates of SaS inside the nth layer are defined as

$$x_3^{(n)1} = x_3^{[n-1]}, \quad x_3^{(n)I_n} = x_3^{[n]},$$
$$x_3^{(n)m_n} = \frac{1}{2}\left(x_3^{[n-1]} + x_3^{[n]}\right) - \frac{1}{2}h_n \cos\left(\pi \frac{2m_n - 3}{2(I_n - 2)}\right), \tag{2}$$

where the index m_n identifies the belonging of any quantity to inner SaS of the nth layer and runs from 2 to $I_n - 1$, whereas the indices i_n, j_n, k_n to be introduced later for describing all SaS of the nth layer run from 1 to I_n.

Remark 1. It is worth noting that transverse coordinates of inner SaS (2) coincide with the nodes of Chebyshev polynomials [25]. This fact has a great meaning for a convergence of the SaS method.

The strain tensor is given by

$$2\varepsilon_{ij} = u_{i,j} + u_{j,i}, \tag{3}$$

where u_i are the displacements of the plate. Here and in the following developments, Latin indices i, j, k, ℓ range from 1 to 3 while Greek indices α, β range from 1 to 2.

The strain components at SaS can be written as

$$2\varepsilon_{\alpha\beta}^{(n)i_n} = 2\varepsilon_{\alpha\beta}\left(x_3^{(n)i_n}\right) = u_{\alpha,\beta}^{(n)i_n} + u_{\beta,\alpha}^{(n)i_n},$$
$$2\varepsilon_{\alpha 3}^{(n)i_n} = 2\varepsilon_{\alpha 3}\left(x_3^{(n)i_n}\right) = \beta_\alpha^{(n)i_n} + u_{3,\alpha}^{(n)i_n}, \tag{4}$$
$$2\varepsilon_{33}^{(n)i_n} = 2\varepsilon_{33}\left(x_3^{(n)i_n}\right) = \beta_3^{(n)i_n},$$

where $u_i^{(n)i_n}(x_1, x_2)$ are the displacements of SaS of the nth layer; $\beta_i^{(n)i_n}(x_1, x_2)$ are the derivatives of displacements with respect to coordinate x_3 at SaS, that is,

$$u_i^{(n)i_n} = u_i\left(x_3^{(n)i_n}\right), \quad \beta_i^{(n)i_n} = u_{i,3}\left(x_3^{(n)i_n}\right). \tag{5}$$

3. Displacement and strain distributions in thickness direction

Up to this moment, no assumptions concerning displacement and strain fields have been made. We start now with the first fundamental assumption of the proposed higher order layer-wise plate theory. Let us assume that the displacements are distributed through the thickness of the nth layer as follows:

$$u_i^{(n)} = \sum_{i_n} L^{(n)i_n} u_i^{(n)i_n}, \quad x_3^{[n-1]} \leqslant x_3 \leqslant x_3^{[n]}, \tag{6}$$

where $L^{(n)i_n}(x_3)$ are the Lagrange polynomials of degree $I_n - 1$ expressed as

$$L^{(n)i_n} = \prod_{j_n \neq i_n} \frac{x_3 - x_3^{(n)j_n}}{x_3^{(n)i_n} - x_3^{(n)j_n}}. \tag{7}$$

The use of Eqs. (5) and (6) yields

$$\beta_i^{(n)i_n} = \sum_{j_n} M^{(n)j_n}\left(x_3^{(n)i_n}\right) u_i^{(n)j_n}, \tag{8}$$

where $M^{(n)j_n} = L_{,3}^{(n)j_n}$ are the derivatives of Lagrange polynomials. The values of these derivatives at SaS of the nth layer are calculated as

$$M^{(n)j_n}\left(x_3^{(n)i_n}\right) = \frac{1}{x_3^{(n)j_n} - x_3^{(n)i_n}} \prod_{k_n \neq i_n j_n} \frac{x_3^{(n)i_n} - x_3^{(n)k_n}}{x_3^{(n)j_n} - x_3^{(n)k_n}} \text{ for } j_n \neq i_n,$$
$$M^{(n)i_n}\left(x_3^{(n)i_n}\right) = -\sum_{j_n \neq i_n} M^{(n)j_n}\left(x_3^{(n)i_n}\right). \tag{9}$$

The latter formula is valid because a useful identity for derivatives of the Lagrange polynomials

$$\sum_{j_n} M^{(n)j_n} = 0 \tag{10}$$

holds. Thus, the key functions $\beta_i^{(n)i_n}$ of the proposed higher order layer-wise plate theory are represented according to (8) as a linear combination of displacements of SaS of the nth layer $u_i^{(n)j_n}$.

The following step consists in a choice of consistent approximation of strains through the thickness of the nth layer. It is apparent that the strain distribution should be chosen similar to the displacement distribution (6), that is,

$$\varepsilon_{ij}^{(n)} = \sum_{i_n} L^{(n)i_n} \varepsilon_{ij}^{(n)i_n}, \quad x_3^{[n-1]} \leqslant x_3 \leqslant x_3^{[n]}. \tag{11}$$

4. Total potential energy of laminated plate

Substituting strains (11) in a formula for the total potential energy and introducing stress resultants

$$H_{ij}^{(n)i_n} = \int_{x_3^{[n-1]}}^{x_3^{[n]}} \sigma_{ij}^{(n)} L^{(n)i_n} dx_3, \tag{12}$$

one obtains

$$\Pi = \int\int_\Omega \left[\frac{1}{2}\sum_n \sum_{i_n} \sum_{i,j} H_{ij}^{(n)i_n} \varepsilon_{ij}^{(n)i_n} - \sum_i \left(p_i^{[N]} u_i^{[N]} - p_i^{[0]} u_i^{[0]}\right)\right] dx_1 dx_2 - W_\Sigma, \tag{13}$$

where $p_i^{[0]}$ and $p_i^{[N]}$ are the loads acting on the bottom and top surfaces $\Omega^{[0]}$ and $\Omega^{[N]}$; W_Σ is the work done by external loads applied to the boundary surface Σ.

For simplicity, we consider the case of linear elastic materials, which are described by the generalized Hooke's law:

$$\sigma_{ij}^{(n)} = \sum_{k,\ell} C_{ijk\ell}^{(n)} \varepsilon_{k\ell}^{(n)}, \quad x_3^{[n-1]} \leqslant x_3 \leqslant x_3^{[n]}, \tag{14}$$

where $C_{ijkl}^{(n)}$ are the components of the material tensor of the nth layer.

Inserting stresses (14) in Eq. (12) and taking into account the strain distribution (11), we have

$$H_{ij}^{(n)i_n} = \sum_{j_n} \sum_{k,\ell} D_{ijk\ell}^{(n)i_n j_n} \varepsilon_{k\ell}^{(n)j_n}, \tag{15}$$

where

$$D_{ijk\ell}^{(n)i_n j_n} = C_{ijk\ell}^{(n)} \int_{x_3^{[n-1]}}^{x_3^{[n]}} L^{(n)i_n} L^{(n)j_n} dx_3. \tag{16}$$

5. Exact 3D solution for laminated orthotropic plates

Consider a simply supported laminated orthotropic rectangular plate subjected to the sinusoidally distributed transverse load

$$p_3^{[N]} = p_0 \sin\frac{\pi x_1}{a} \sin\frac{\pi x_2}{b}, \tag{17}$$

where a and b are the plate dimensions. To satisfy the boundary conditions, we search the analytical solution of the problem as follows:

$$\begin{aligned} &u_1^{(n)i_n} = u_{10}^{(n)i_n} \cos\frac{\pi x_1}{a} \sin\frac{\pi x_2}{b}, \quad u_2^{(n)i_n} = u_{20}^{(n)i_n} \sin\frac{\pi x_1}{a} \cos\frac{\pi x_2}{b}, \\ &u_3^{(n)i_n} = u_{30}^{(n)i_n} \sin\frac{\pi x_1}{a} \sin\frac{\pi x_2}{b}. \end{aligned} \tag{18}$$

Substituting Eqs. (17) and (18) into the total potential energy (13) with $W_\Sigma = 0$ and allowing for Eqs. (4), (8) and (15), one finds

$$\Pi = \Pi\left(u_{i0}^{(n)i_n}\right). \tag{19}$$

Invoking further the principle of the minimum total potential energy, we arrive at the system of linear algebraic equations

$$\frac{\partial \Pi}{\partial u_{i0}^{(n)i_n}} = 0 \tag{20}$$

of order $3(\sum_n I_n - N + 1)$. The linear system (20) can be easily solved by using a method of Gaussian elimination.

The described algorithm was performed with the Symbolic Math Toolbox, which incorporates symbolic computations into the numeric environment of MATLAB. The latter gave the possibility to derive the exact solutions of 3D elasticity for laminated orthotropic plates with a prescribed accuracy.

5.1. Rectangular three-ply composite plate

The mechanical and geometrical parameters of the plate are taken to be $E_L = 25E_T$, $G_{LT} = 0.5E_T$, $G_{TT} = 0.2E_T$, $E_T = 10^6$, $\nu_{LT} = \nu_{TT} = 0.25$, $b = 3a$ and $h_n = h/3$, where subscripts L and T refer to the fiber and transverse ply directions. Here, we consider a symmetric three-ply laminate with a stacking sequence [0/90/0]. To compare the results with Pagano's exact solution [27], the following dimensionless variables are introduced:

$$\begin{aligned} &U_3 = 100E_T h^3 u_3(a/2, b/2, z)/p_0 a^4, \quad S_{11} = h^2 \sigma_{11}(a/2, b/2, z)/p_0 a^2, \\ &S_{22} = 10h^2 \sigma_{22}(a/2, b/2, z)/p_0 a^2, \quad S_{12} = 10h^2 \sigma_{12}(0, 0, z)/p_0 a^2, \\ &S_{13} = 10h\sigma_{13}(0, b/2, z)/p_0 a, \quad S_{23} = 10h\sigma_{23}(a/2, 0, z)/p_0 a, \\ &S_{33} = \sigma_{33}(a/2, b/2, z)/p_0, \quad z = x_3/h. \end{aligned} \tag{21}$$

The data listed in Tables 1–3 show that the SaS technique allows one to derive the exact 3D solutions even for very thick plates with a prescribed accuracy using a large number of SaS. Fig. 2 presents the distribution of transverse shear stresses in

Table 1
Results for a symmetric three-ply plate with $a/h = 2$.

I_n	$U_3(0)$	$S_{11}(-0.5)$	$S_{11}(0.5)$	$S_{22}(-1/6)$	$S_{22}(1/6)$	$10S_{12}(-0.5)$	$10S_{12}(0.5)$	$S_{13}(0)$	$10S_{23}(0)$	$S_{33}(0.5)$
3	7.9111	−1.4606	1.9265	−2.5925	2.2172	5.2232	−5.3440	2.4423	5.7275	1.0349
4	8.1616	−1.6211	2.1292	−2.6759	2.2940	5.4760	−5.6306	2.5711	6.6814	1.0371
5	8.1648	−1.6236	2.1325	−2.6768	2.2950	5.4808	−5.6364	2.5703	6.6846	1.0037
6	8.1659	−1.6241	2.1332	−2.6772	2.2952	5.4818	−5.6375	2.5709	6.6778	1.0019
7	8.1659	−1.6241	2.1332	−2.6772	2.2952	5.4818	−5.6375	2.5709	6.6778	1.0001
Pagano	8.17	−1.62	2.13	−2.68	2.30	5.48	−5.64	2.57	6.68	1.0000

Table 2
Results for a symmetric three-ply plate with $a/h = 4$.

I_n	$U_3(0)$	$S_{11}(-0.5)$	$S_{11}(0.5)$	$S_{22}(-1/6)$	$S_{22}(1/6)$	$10S_{12}(-0.5)$	$10S_{12}(0.5)$	$S_{13}(0)$	$10S_{23}(0)$	$S_{33}(0.5)$
3	2.7983	−1.0824	1.1269	−1.1834	1.0790	2.7777	−2.6586	3.4719	2.9304	1.0505
4	2.8210	−1.0994	1.1445	−1.1929	1.0878	2.8063	−2.6876	3.5108	3.3372	1.0207
5	2.8211	−1.0992	1.1443	−1.1929	1.0878	2.8065	−2.6878	3.5108	3.3374	1.0012
6	2.8211	−1.0992	1.1443	−1.1929	1.0878	2.8065	−2.6878	3.5108	3.3365	1.0003
7	2.8211	−1.0992	1.1443	−1.1929	1.0878	2.8065	−2.6878	3.5108	3.3365	1.0000
Pagano	2.82	−1.10	1.14	−1.19	1.09	2.81	−2.69	3.51	3.34	1.0000

Table 3
Results for a symmetric three-ply plate with $a/h = 100$.

I_n	$U_3(0)$	$S_{11}(-0.5)$	$S_{11}(0.5)$	$S_{22}(-1/6)$	$S_{22}(1/6)$	$10S_{12}(-0.5)$	$10S_{12}(0.5)$	$S_{13}(0)$	$10S_{23}(0)$	$S_{33}(0.5)$
3	0.50766	−0.62436	0.62435	−0.25326	0.25308	0.83223	−0.83192	4.3853	0.9893	1.0641
4	0.50766	−0.62436	0.62435	−0.25236	0.25308	0.83224	−0.83192	4.3932	1.0836	1.0064
5	0.50766	−0.62436	0.62435	−0.25236	0.25308	0.83224	−0.83192	4.3932	1.0836	1.0000
Pagano	0.508	−0.624	0.624	−0.253	0.253	0.83	−0.83	4.39	1.08	1.0000

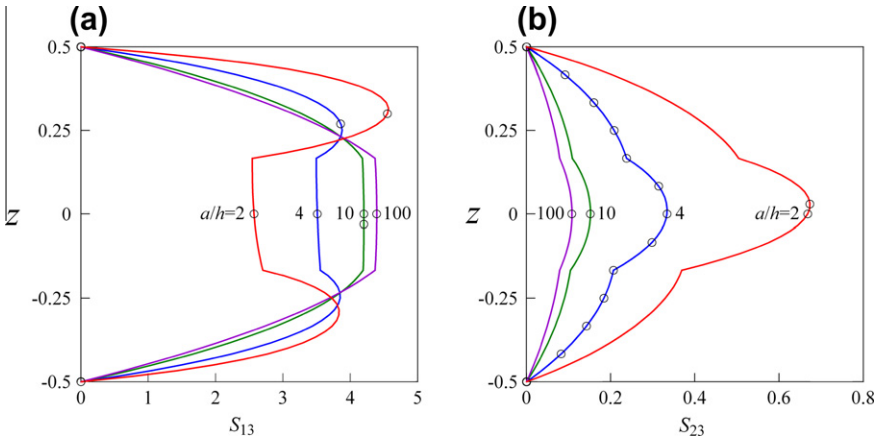

Fig. 2. Distribution of transverse shear stresses S_{13} and S_{23} through the thickness of the three-ply plate for $I_1 = I_2 = I_3 = 7$: present analysis (—) and Pagano (○).

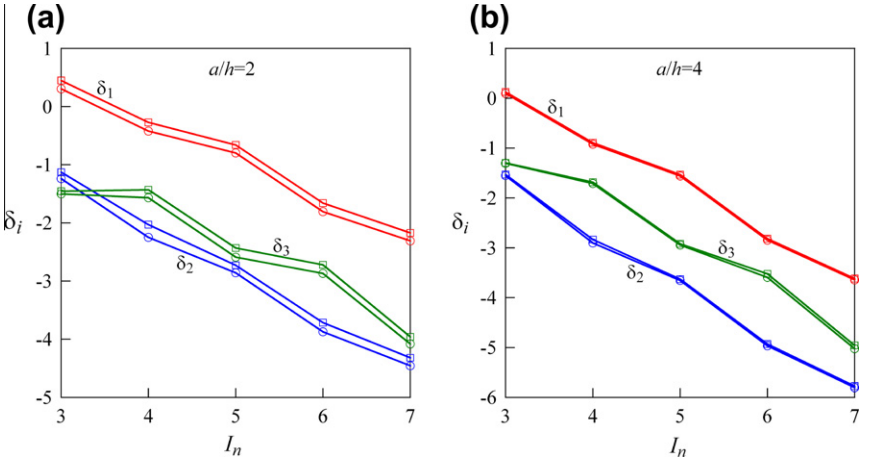

Fig. 3. Accuracy of satisfying the boundary conditions $\delta_i(-h/2)$ and $\delta_i(h/2)$ on the bottom (○) and top (□) surfaces of the three-ply plate: (a) $a/h = 2$ and (b) $a/h = 4$, where $\delta_i = \lg\left|S_{i3}^{3D} - S_{i3}\right|$.

the thickness direction for different values of the slenderness ratio a/h by choosing seven SaS for each layer. These results demonstrate convincingly the high potential of the proposed layer-wise plate formulation. This is due to the fact that boundary conditions on the bottom and top surfaces and continuity conditions at layer interfaces for transverse shear stresses are satisfied precisely without integration of the equilibrium equations of elasticity. Fig. 3 displays the logarithmic errors $\delta_i(-h/2)$ and $\delta_i(h/2)$, which help to assess the accuracy of fulfilling the boundary conditions for transverse stresses on the bottom and top surfaces of the

Table 4
Results for a sandwich plate with $a/h = 2$.

I_n	$S_{11}(-0.5)$	$S_{11}(-0.4)$	$S_{11}(0.4)$	$S_{11}(0.5)$	$S_{22}(-0.5)$	$S_{22}(0.5)$	$S_{12}(-0.5)$	$S_{12}(0.5)$	$S_{13}(0)$	$S_{23}(0)$	$S_{33}(0.5)$
3	−2.6438	1.6599	−2.2105	3.2682	−3.9177	4.5167	2.3308	−2.3955	1.8174	1.3539	1.0170
4	−2.6531	1.6684	−2.2205	3.2787	−3.9232	4.5227	2.3378	−2.4028	1.8484	1.3990	1.0085
5	−2.6525	1.6679	−2.2199	3.2781	−3.9190	4.5174	2.3378	−2.4028	1.8483	1.3990	1.0001
6	−2.6525	1.6679	−2.2199	3.2781	−3.9190	4.5173	2.3378	−2.4028	1.8480	1.3986	1.0000
7	−2.6525	1.6679	−2.2199	3.2781	−3.9190	4.5173	2.3378	−2.4028	1.8480	1.3986	1.0000
Pagano	−2.653	1.668	−2.220	3.278	−3.919	4.517	2.338	−2.403	1.85	1.399	1.0000

Table 5
Results for a sandwich plate with $a/h = 4$.

I_n	$S_{11}(-0.5)$	$S_{11}(-0.4)$	$S_{11}(0.4)$	$S_{11}(0.5)$	$S_{22}(-0.5)$	$S_{22}(0.5)$	$S_{12}(-0.5)$	$S_{12}(0.5)$	$S_{13}(0)$	$S_{23}(0)$	$S_{33}(0.5)$
3	−1.5118	0.19588	−0.23271	1.5556	−2.5344	2.5966	1.4800	−1.4361	2.3710	1.0452	1.0165
4	−1.5121	0.19633	−0.23317	1.5559	−2.5331	2.5953	1.4805	−1.4366	2.3867	1.0720	1.0028
5	−1.5121	0.19628	−0.23311	1.5558	−2.5327	2.5949	1.4805	−1.4366	2.3867	1.0720	1.0000
6	−1.5121	0.19628	−0.23311	1.5558	−2.5327	2.5949	1.4805	−1.4366	2.3867	1.0719	1.0000
7	−1.5121	0.19628	−0.23311	1.5558	−2.5327	2.5949	1.4805	−1.4366	2.3867	1.0719	1.0000
Pagano	−1.512	0.196	−0.233	1.556	−2.533	2.595	1.481	−1.437	2.39	1.072	1.0000

Table 6
Results for a sandwich plate with $a/h = 100$.

I_n	$S_{11}(-0.5)$	$S_{11}(-0.4)$	$S_{11}(0.4)$	$S_{11}(0.5)$	$S_{22}(-0.5)$	$S_{22}(0.5)$	$S_{12}(-0.5)$	$S_{12}(0.5)$	$S_{13}(0)$	$S_{23}(0)$	$S_{33}(0.5)$
3	−1.0975	−0.87482	0.87482	1.0975	−0.54960	0.54965	0.43667	−0.43657	3.2333	0.29141	1.0157
4	−1.0975	−0.87482	0.87482	1.0975	−0.54960	0.54964	0.43667	−0.43657	3.2400	0.29744	1.0004
5	−1.0975	−0.87482	0.87482	1.0975	−0.54960	0.54964	0.43667	−0.43657	3.2400	0.29744	1.0000
Pagano	−1.098	−0.875	0.875	1.098	−0.550	0.550	0.437	−0.437	3.24	0.297	1.0000

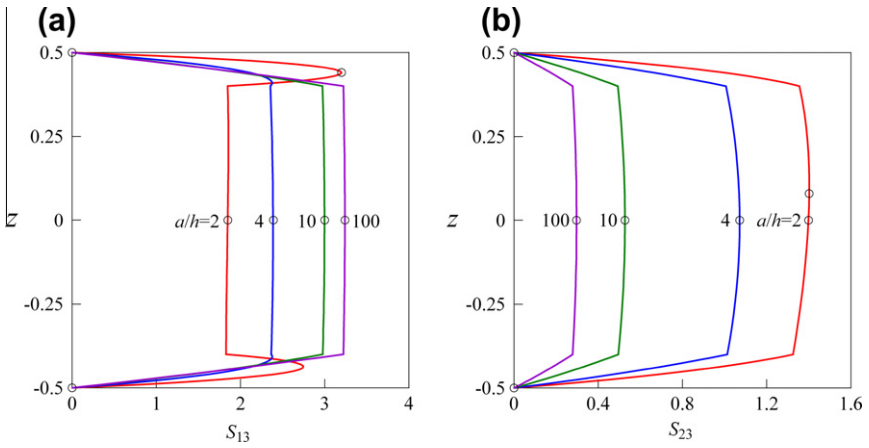

Fig. 4. Distribution of transverse shear stresses S_{13} and S_{23} through the thickness of the sandwich plate for $I_1 = I_2 = I_3 = 7$: present analysis (—) and Pagano (○).

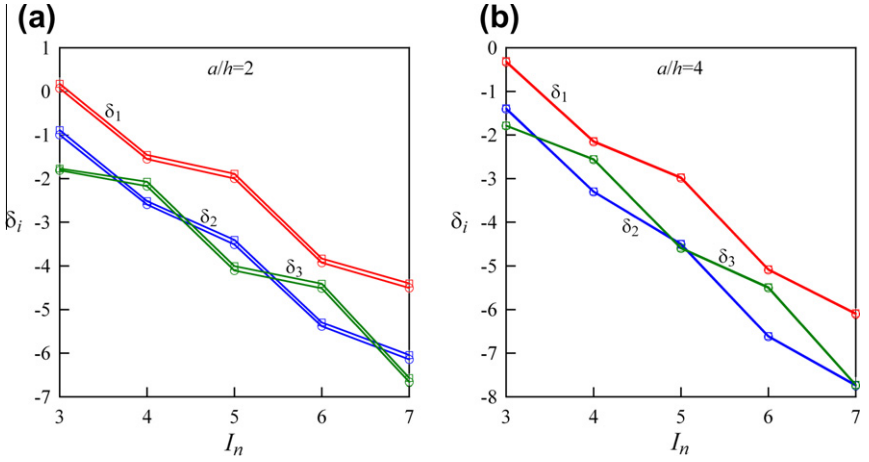

Fig. 5. Accuracy of satisfying the boundary conditions $\delta_i(-h/2)$ and $\delta_i(h/2)$ on the bottom (○) and top (□) surfaces of the sandwich plate: (a) $a/h = 2$ and (b) $a/h = 4$, where $\delta_i = \lg\left|S_{i3}^{3D} - S_{i3}\right|$.

plate. It is necessary to note that the proposed SaS method provides a monotonic convergence that is impossible with *equally spaced* SaS.

5.2. Square sandwich plate

Next, we study a simply supported square sandwich plate with ply thicknesses $h_1 = h_3 = 0.1h$ and $h_2 = 0.8h$. The face sheets are made of the unidirectional composite given in a previous section. The mechanical properties of the core are taken to be $E_1 = E_2 = 4 \cdot 10^4$, $E_3 = 5 \cdot 10^5$, $G_{13} = G_{23} = 6 \cdot 10^4$, $G_{12} = 1.6 \cdot 10^4$, $\nu_{31} = \nu_{32} = \nu_{12} = 0.25$. The results derived are compared with Pagano's exact solution [27] through the use of dimensionless variables (21) by setting $b = a$.

Tables 4–6 demonstrate again the high potential of the layer-wise plate formulation developed. Fig. 4 shows the distribution of transverse shear stresses in the thickness direction for different slenderness ratios choosing seven SaS for each layer. It is seen that boundary conditions on the bottom and top surfaces are satisfied properly in spite of applying the constitutive Eq. (14). To confirm this statement, we represent in Fig. 5 the accuracy of fulfilling the boundary conditions for transverse stresses on the bottom and top surfaces of the plate.

6. Exact 3D solution for laminated anisotropic plates in cylindrical bending

Consider a simply supported laminated anisotropic plate in cylindrical bending subjected to the sinusoidal transverse load

$$p_3^{[N]} = p_0 \sin\frac{\pi x_1}{a}, \tag{22}$$

where a is the width of the plate.

To satisfy the boundary conditions, we search the analytical solution of the problem as follows:

$$u_1^{(n)i_n} = u_{10}^{(n)i_n}\cos\frac{\pi x_1}{a}, \quad u_2^{(n)i_n} = u_{20}^{(n)i_n}\cos\frac{\pi x_1}{a}, \quad u_3^{(n)i_n} = u_{30}^{(n)i_n}\sin\frac{\pi x_1}{a}. \tag{23}$$

Substituting (22) and (23) in the total potential energy (13) and invoking the principle of the minimum total potential energy, we obtain the system of linear algebraic Eq. (20). This system is solved by a method of Gaussian elimination. The described algorithm was performed with the Symbolic Math Toolbox, which incorporates symbolic computations into the numeric environment of MATLAB.

6.1. Angle-ply laminated composite plate

Consider a symmetric three-layer composite plate with ply thicknesses $h_1 = h_3 = h/4$ and $h_2 = h/2$ and stacking sequence [30/−30/30]. The material properties of the unidirectional composite are presented in Section 5.1. To compare the results derived with Pagano's exact solution [31], the following dimensionless variables are introduced:

$$\begin{aligned} &U_3 = 100E_T h^3 u_3(a/2,z)/p_0 a^4,\\ &S_{11} = 10h^2\sigma_{11}(a/2,z)/p_0 a^2, \quad S_{12} = 10h^2\sigma_{12}(0,z)/p_0 a^2,\\ &S_{\alpha 3} = 10h\sigma_{\alpha 3}(0,z)/p_0 a, \quad S_{33} = \sigma_{33}(a/2,z)/p_0, \quad z = \theta_3/h. \end{aligned} \tag{24}$$

The data listed in Tables 7–9 show that the SaS technique permits the derivation of exact solutions of plane strain elasticity even for thick angle-ply plates with a prescribed accuracy using a large number of SaS. Fig. 6 presents the distribution of transverse shear stresses in the thickness direction for different values of the slenderness ratio a/h by choosing seven SaS for each layer. As can be seen, the boundary conditions on the bottom and top surfaces and continuity conditions at layer interfaces for transverse stresses are satisfied with a high accuracy applying again constitutive Eq. (14). This statement is confirmed convincingly by Fig. 7. It should be mentioned that the proposed SaS method provides the uniform convergence for angle-ply plates that is impossible with *equally spaced* SaS [21].

7. Exact 3D solution for antisymmetric angle-ply plate

Consider a simply supported antisymmetric angle-ply rectangular plate subjected to the sinusoidally distributed transverse load

$$p_3^{[0]} = -\frac{1}{2}p_0\sin\frac{\pi x_1}{a}\sin\frac{\pi x_2}{b}, \quad p_3^{[N]} = \frac{1}{2}p_0\sin\frac{\pi x_1}{a}\sin\frac{\pi x_2}{b} \tag{25}$$

and search the analytical solution of the problem in the following form:

$$\begin{aligned} u_1^{(n)i_n} &= \bar{u}_{10}^{(n)i_n}\cos\frac{\pi x_1}{a}\sin\frac{\pi x_2}{b} + \tilde{u}_{10}^{(n)i_n}\sin\frac{\pi x_1}{a}\cos\frac{\pi x_2}{b},\\ u_2^{(n)i_n} &= \bar{u}_{20}^{(n)i_n}\sin\frac{\pi x_1}{a}\cos\frac{\pi x_2}{b} + \tilde{u}_{20}^{(n)i_n}\cos\frac{\pi x_1}{a}\sin\frac{\pi x_2}{b},\\ u_3^{(n)i_n} &= \bar{u}_{30}^{(n)i_n}\sin\frac{\pi x_1}{a}\sin\frac{\pi x_2}{b} + \tilde{u}_{30}^{(n)i_n}\cos\frac{\pi x_1}{a}\cos\frac{\pi x_2}{b}. \end{aligned} \tag{26}$$

Substituting Eqs. (25) and (26) into the total potential energy (13) with $W_\Sigma = 0$ and taking into account relations (4), (8) and (15), we obtain

$$\Pi = \Pi\left(\bar{u}_{i0}^{(n)i_n}, \tilde{u}_{i0}^{(n)i_n}\right). \tag{27}$$

Invoking the principle of the minimum total potential energy, one arrives at the system of linear algebraic equations

$$\frac{\partial\Pi}{\partial\bar{u}_{i0}^{(n)i_n}} = 0, \quad \frac{\partial\Pi}{\partial\tilde{u}_{i0}^{(n)i_n}} = 0 \tag{28}$$

of order $6(\sum_n I_n - N + 1)$. The linear system (28) is solved using a method of Gaussian elimination. The described algorithm was performed with the help of the Symbolic Math Toolbox.

Table 7
Results for an angle-ply plate with $a/h = 2$.

I_n	$U_3(-0.5)$	$U_3(0)$	$U_3(0.5)$	$S_{11}(0.5)$	$S_{12}(0.5)$	$S_{13}(0)$	$S_{23}(0.3)$	$S_{33}(0.5)$
3	7.9961	8.6849	10.855	14.499	−6.6104	4.0347	−1.0567	1.0289
5	8.2414	8.9154	11.104	15.180	−6.9178	4.6995	−1.0003	1.0011
7	8.2432	8.9178	11.106	15.183	−6.9189	4.6296	−1.0106	1.0000
9	8.2432	8.9178	11.106	15.183	−6.9189	4.6330	−1.0106	1.0000
11	8.2432	8.9178	11.106	15.183	−6.9189	4.6329	−1.0106	1.0000

Table 8
Results for an angle-ply plate with $a/h = 4$.

I_n	$U_3(-0.5)$	$U_3(0)$	$U_3(0.5)$	$S_{11}(0.5)$	$S_{12}(0.5)$	$S_{13}(0)$	$S_{23}(0.3)$	$S_{33}(0.5)$
3	3.1923	3.2531	3.2531	8.3971	−4.0226	4.3664	−1.2610	1.0327
5	3.2305	3.2900	3.4138	8.5205	−4.0811	5.0215	−1.2566	1.0003
7	3.2306	3.2901	3.4138	8.5205	−4.0811	5.0019	−1.2578	1.0000
9	3.2306	3.2901	3.4138	8.5205	−4.0811	5.0022	−1.2578	1.0000
11	3.2306	3.2901	3.4138	8.5205	−4.0811	5.0022	−1.2578	1.0000

Table 9
Results for an angle-ply plate with $a/h = 100$.

I_n	$U_3(-0.5)$	$U_3(0)$	$U_3(0.5)$	$S_{11}(0.5)$	$S_{12}(0.5)$	$S_{13}(0)$	$S_{23}(0.3)$	$S_{33}(0.5)$
3	0.84662	0.84665	0.84662	6.0831	−3.2257	4.3804	−1.6241	1.0393
5	0.84663	0.84666	0.84663	6.0832	−3.2258	4.7758	−1.6199	1.0000
7	0.84663	0.84666	0.84663	6.0832	−3.2258	4.7758	−1.6199	1.0000

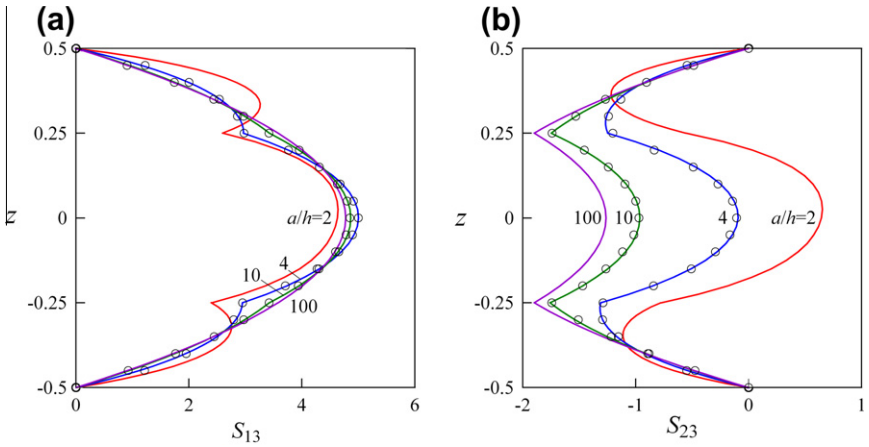

Fig. 6. Distribution of transverse shear stresses S_{13} and S_{23} through the thickness of the angle-ply plate for $I_1 = I_2 = I_3 = 7$: present analysis (—) and Pagano (○).

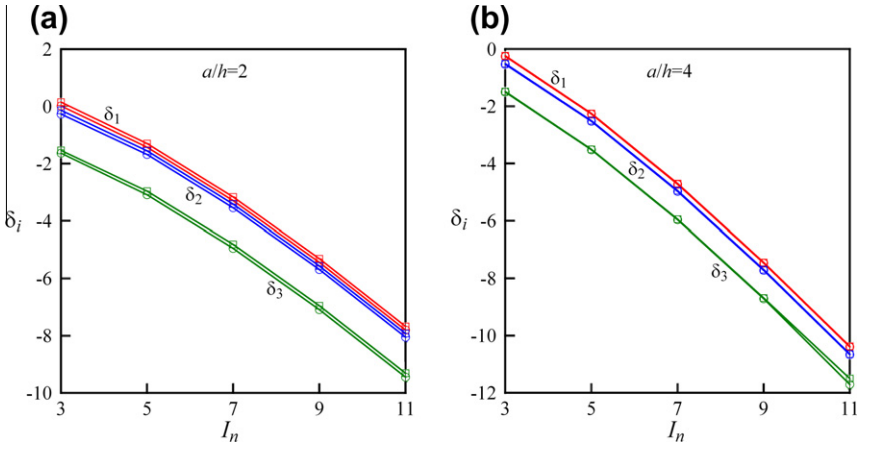

Fig. 7. Accuracy of satisfying the boundary conditions $\delta_i(-h/2)$ and $\delta_i(h/2)$ on the bottom (○) and top (□) surfaces of the angle-ply plate: (a) $a/h = 2$ and (b) $a/h = 4$, where $\delta_i = \lg\left|S_{i3}^{3D} - S_{i3}\right|$.

7.1. Unsymmetric two-layer angle-ply composite plate

Consider unsymmetric angle-ply square and rectangular plates with two layers of equal thicknesses and stacking sequence [−15/15]. The plate dimensions are taken to be $b = a$ and $b = 3a$. The plies are made of the unidirectional composite presented in Section 5.1. To compare the results with Savoia-Reddy's exact 3D solution [33], we introduce the following dimensionless variables:

$$U_3 = 100E_T h^3 u_3(a/2,b/2,z)/p_0 a^4, \quad S_{\alpha\beta} = 10h^2\sigma_{\alpha\beta}(a/2,b/2,z)/p_0 a^2,$$
$$\overline{S}_{13} = 10h\sigma_{13}(0,b/2,z)/p_0 a, \quad \widetilde{S}_{13} = 10h\sigma_{13}(a/2,0,z)/p_0 a,$$
$$\overline{S}_{23} = 10h\sigma_{23}(a/2,0,z)/p_0 a, \quad \widetilde{S}_{23} = 10h\sigma_{23}(0,b/2,z)/p_0 a,$$
$$S_{33} = \sigma_{33}(a/2,b/2,z)/p_0, \quad z = x_3/h. \tag{29}$$

Tables 10–12 show the high potential of the proposed layer-wise formulation based on the SaS technique for derivation of exact 3D elasticity solutions for unsymmetric angle-ply laminates. Fig. 8 displays the distribution of transverse shear stresses (29) in the thickness direction for different slenderness ratios by choosing seven SaS for each layer. It is seen that boundary conditions on the bottom and top surfaces and continuity conditions at the layer interface are satisfied correctly in spite of applying the constitutive equations (14). To confirm this statement, we represent in Fig. 9 the accuracy of fulfilling the boundary conditions for transverse stresses on the top surface of the laminate through the use of logarithmic errors $\bar{\delta}_\alpha = \lg\left|\overline{S}_{\alpha 3}^{3D} - \overline{S}_{\alpha 3}\right|$, $\tilde{\delta}_\alpha = \lg\left|\widetilde{S}_{\alpha 3}^{3D} - \widetilde{S}_{\alpha 3}\right|$ and $\delta_3 = \lg\left|S_{33}^{3D} - S_{33}\right|$.

Table 10
Results for a square unsymmetric angle-ply plate with $a/h = 4$.

I_n	$U_3(0)$	$S_{11}(0.5)$	$S_{22}(0.5)$	$S_{12}(0.5)$	$\overline{S}_{13}(0.145)$	$\overline{S}_{23}(0.125)$	$\widetilde{S}_{13}(-0.280)$	$\widetilde{S}_{23}(-0.280)$
3	1.6599	6.2113	1.0939	1.3794	2.9233	0.92325	0.64420	0.29546
5	1.7057	6.6441	1.1354	1.4883	3.1333	0.95559	0.85778	0.40460
7	1.7059	6.6448	1.1350	1.4889	3.1453	0.96051	0.84054	0.39872
9	1.7059	6.6447	1.1350	1.4886	3.1447	0.96037	0.84091	0.39883
11	1.7059	6.6447	1.1350	1.4886	3.1447	0.96037	0.84091	0.39883
Savoia	1.7059	6.645	1.135	1.489	3.145	0.960	0.841	0.399

Table 11
Results for a square unsymmetric angle-ply plate with $a/h = 10$.

I_n	$U_3(0)$	$S_{11}(0.5)$	$S_{22}(0.5)$	$S_{12}(0.5)$	$\bar{S}_{13}(0.140)$	$\bar{S}_{23}(0.150)$	$\tilde{S}_{13}(-0.255)$	$\tilde{S}_{23}(-0.255)$
3	0.79540	5.5700	0.79976	1.2292	3.1966	0.74412	0.68261	0.28161
5	0.80272	5.6332	0.80620	1.2440	3.4185	0.81342	0.99495	0.41292
7	0.80272	5.6331	0.80618	1.2440	3.4209	0.81379	0.99112	0.41168
9	0.80272	5.6331	0.80618	1.2440	3.4209	0.81378	0.99113	0.41169
11	0.80272	5.6331	0.80618	1.2440	3.4209	0.81378	0.99113	0.41169
Savoia	0.8027	5.633	0.806	1.244	3.421	0.8138	0.9911	0.412

Table 12
Results for a rectangular unsymmetric angle-ply plate with $a/h = 4$.

I_n	$U_3(0)$	$S_{11}(0.5)$	$S_{22}(0.5)$	$S_{12}(0.5)$	$\bar{S}_{13}(0.175)$	$\bar{S}_{23}(0.145)$	$\tilde{S}_{13}(-0.270)$	$\tilde{S}_{23}(-0.270)$
3	2.4164	9.0190	0.87325	1.8927	3.4629	0.33657	0.34499	0.42701
5	2.4902	9.5801	0.91178	2.0182	3.9911	0.36344	0.46567	0.59813
7	2.4903	9.5804	0.91142	2.0184	3.9877	0.36476	0.45641	0.59110
9	2.4903	9.5804	0.91140	2.0184	3.9875	0.36470	0.45660	0.59121
11	2.4903	9.5804	0.91140	2.0184	3.9875	0.36470	0.45660	0.59121
Savoia	2.4903	9.581	0.911	2.018	3.988	0.365	0.457	0.591

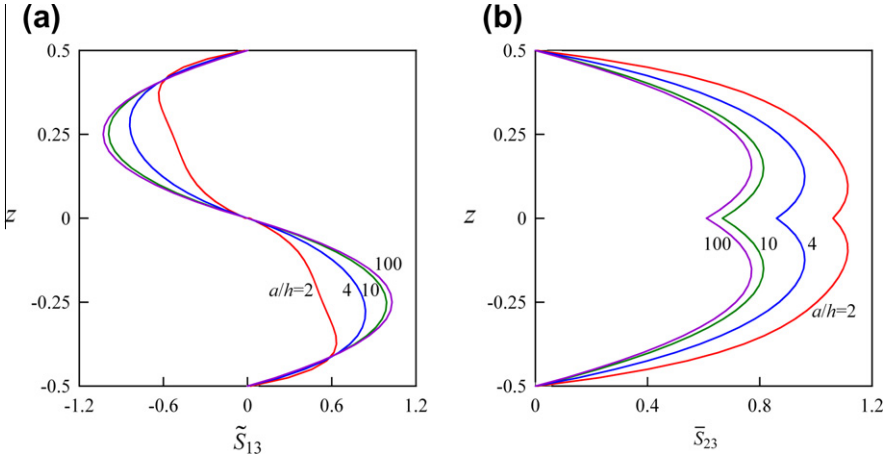

Fig. 8. Distribution of transverse shear stresses: (a) $\tilde{S}_{13}$ and (b) $\bar{S}_{23}$ through the thickness of the square unsymmetric angle-ply plate for $I_1 = I_2 = 7$.

Table 13
Results for a sandwich plate with angle-ply face sheets ($a/h = 4$).

I_n	$U_3(0)$	$S_{11}(0.5)$	$S_{22}(0.5)$	$S_{12}(0.5)$	$\bar{S}_{13}(0.407)$	$\bar{S}_{23}(0)$	$\tilde{S}_{13}(0.444)$	$\tilde{S}_{23}(0.444)$
3	5.7781	8.1571	3.5991	−0.10854	2.1597	1.4754	−0.020872	−0.014163
5	5.7794	8.1578	3.5978	−0.10806	1.9305	1.4868	−0.033258	−0.020813
7	5.7794	8.1578	3.5977	−0.10806	1.9305	1.4868	−0.033379	−0.020890
9	5.7794	8.1578	3.5977	−0.10806	1.9305	1.4868	−0.033379	−0.020890

Table 14
Results for a sandwich plate with angle-ply face sheets ($a/h = 10$).

I_n	$U_3(0)$	$S_{11}(0.5)$	$S_{22}(0.5)$	$S_{12}(0.5)$	$\bar{S}_{13}(0)$	$\bar{S}_{23}(0)$	$\tilde{S}_{13}(0.442)$	$\tilde{S}_{23}(0.442)$
3	1.4273	5.5263	2.2272	−0.013814	2.1411	1.3601	−0.0030536	−0.0020077
5	1.4273	5.5258	2.2267	−0.013811	2.1453	1.3654	−0.0043692	−0.0027815
7	1.4273	5.5258	2.2267	−0.013811	2.1453	1.3654	−0.0043741	−0.0027846
9	1.4273	5.5258	2.2267	−0.013811	2.1453	1.3654	−0.0043741	−0.0027846

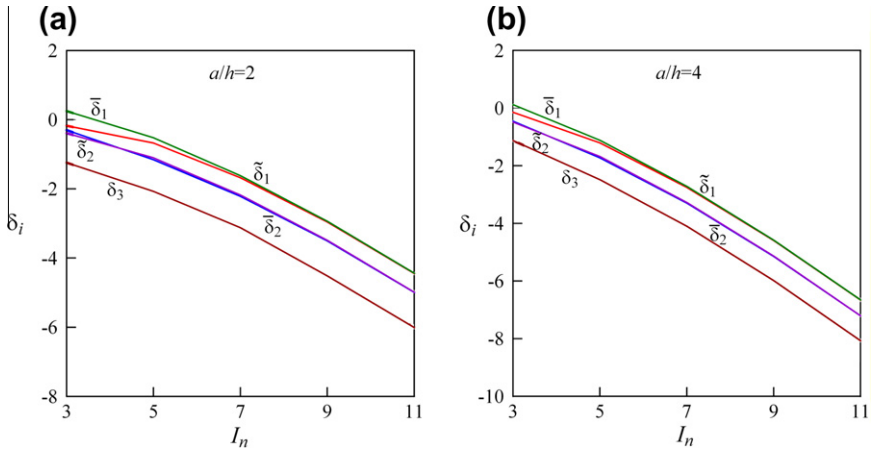

Fig. 9. Accuracy of satisfying boundary conditions $\bar{\delta}_\alpha(h/2)$, $\tilde{\delta}_\alpha(h/2)$ and $\delta_3(h/2)$ on the top surface of the square unsymmetric angle-ply plate: (a) $a/h = 2$ and (b) $a/h = 4$.

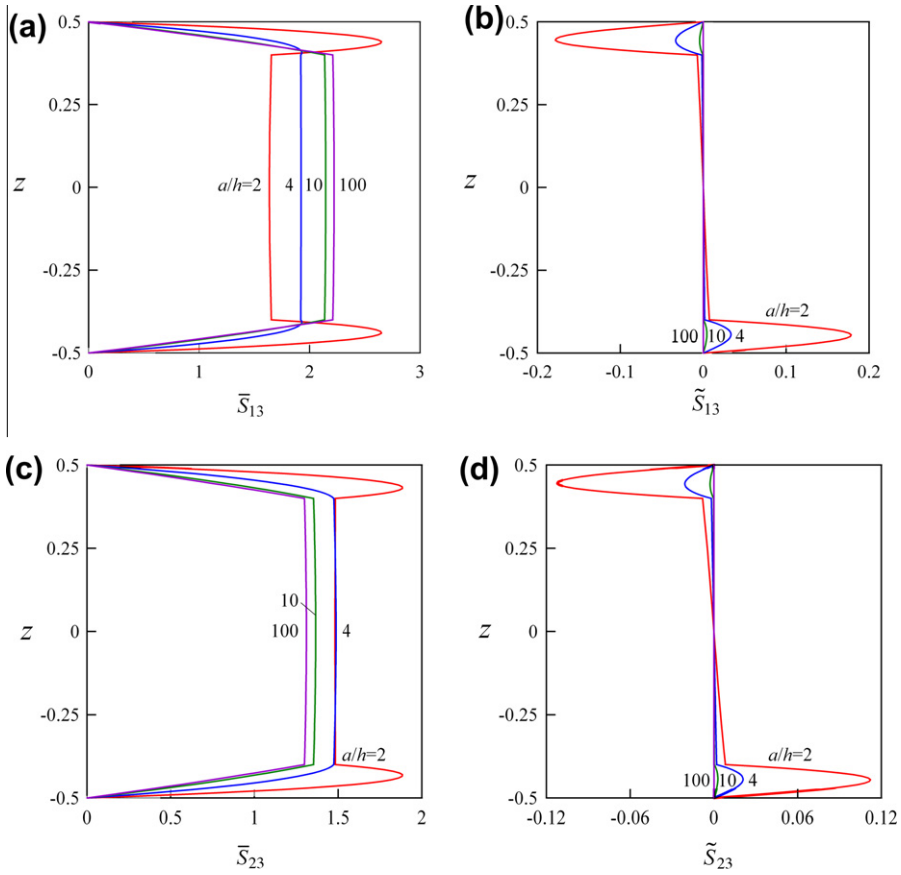

Fig. 10. Distribution of transverse shear stresses through the thickness of the sandwich plate with angle-ply face sheets for $I_1 = I_2 = I_3 = 7$.

7.2. Sandwich plate with antisymmetric angle-ply face sheets

Finally, we study a square sandwich plate with ply thicknesses $h_1 = h_3 = 0.1h$ and $h_2 = 0.8h$ and stacking sequence $[-30/core/30]$. The material properties of the core and face sheets are the same as those in Section 5.2.

Tables 13 and 14 demonstrate the results of the convergence study utilizing a various number of SaS for thick and moderately thick sandwich plates. As expected, $\bar{u}_{30}^{(n)i_n}$ are the values of any even through-the-thickness function while $\tilde{u}_{30}^{(n)i_n}$ are the values of any odd function. Fig. 10 shows the distribution of transverse shear stresses (29) in the thickness direction for different slenderness ratios employing seven SaS for each layer. It is seen that boundary conditions on the bottom and top surfaces and continuity conditions at layer interfaces for transverse stresses are fulfilled properly. This is illustrated by means of Fig. 11, where $\bar{\delta}_\alpha$, $\tilde{\delta}_\alpha$ and δ_3 are the logarithmic errors defined in a previous section.

8. Conclusions

An efficient method of solving the 3D elasticity problems for laminated composite plates has been proposed. It is based on the

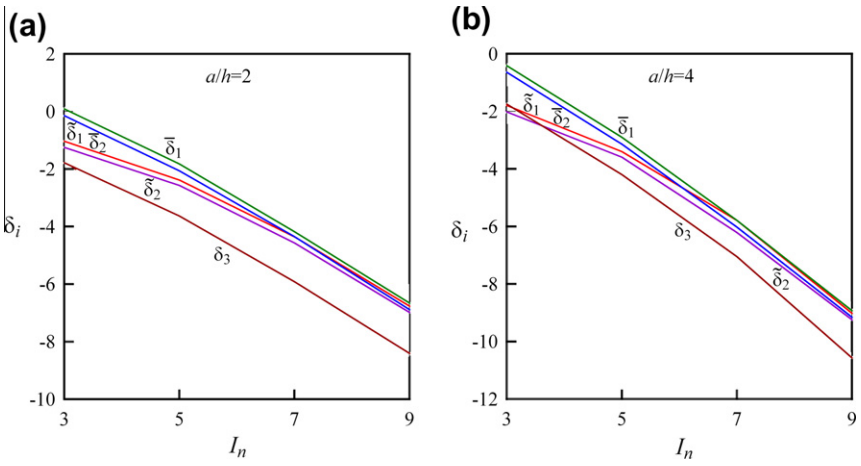

Fig. 11. Accuracy of satisfying the boundary conditions $\bar{\delta}_\alpha(h/2)$, $\tilde{\delta}_\alpha(h/2)$ and $\delta_3(h/2)$ on the top surface of the sandwich plate with angle-ply face sheets: (a) $a/h = 2$ and (b) $a/h = 4$.

new technique of SaS located at the Chebyshev polynomial nodes inside the plate body and layer interfaces as well. The stress analysis of composite plates is based on the 3D constitutive equations and gives an opportunity to obtain the exact 3D solutions of elasticity for thick and thin cross-ply and angle-ply laminates with a prescribed accuracy.

Acknowledgement

This work was partially supported by Russian Ministry of Education and Science under Grant No. 1.472.2011.

References

[1] Carrera E. Theories and finite elements for multilayered plates and shells: a unified compact formulation with numerical assessment and benchmarking. Arch Comp Meth Eng 2003;10:215–96.
[2] Grigolyuk EI, Chulkov PP. Theory of viscoelastic multilayered shells with stiff cores at finite deflections. J Appl Mech Tech Phys 1964;5(5):109–17.
[3] Grigolyuk EI, Chulkov PP. On the theory of multilayered shells. In: Contributions to the theory of aircraft structures. Delft: University Press; 1972. p. 171–83.
[4] Srinivas S. A refined analysis of composite laminates. J Sound Vib 1973;30:495–507.
[5] Librescu L. Improved linear theory of elastic anisotropic multilayered shells, part 1. Mech Comp Mater 1975;11:885–96.
[6] Librescu L. Improved linear theory of elastic anisotropic multilayered shells, part 2. Mech Comp Mater 1976;12:82–90.
[7] Epstein M, Glockner PG. Nonlinear analysis of multilayered shells. Int J Solids Struct 1977;13:1081–9.
[8] Grigolyuk EI, Kulikov GM. Toward a theory of elastic laminated anisotropic shells. Sov Phys Doklady 1984;29:344–5.
[9] Grigolyuk EI, Kulikov GM. General direction of development of the theory of multilayered shells. Mech Comp Mater 1988;24:231–41.
[10] Reddy JN. On the generalization of displacement-based laminate theories. Appl Mech Rev 1989;42:S213–22.
[11] Cho KN, Bert CW, Striz AG. Free vibrations of laminated rectangular plates analyzed by higher order individual-layer theory. J Sound Vib 1991;145:429–42.
[12] Reddy JN. Mechanics of laminated composite plates and shells: theory and analysis. 2nd ed. Boca Raton: CRC Press; 2004.
[13] Grigolyuk EI, Kogan EA. State of the art of the theory of multilayer shells. Int Appl Mech 1972;8:583–95.
[14] Noor AK, Burton WS. Assessment of computational models for multilayered composite shells. Appl Mech Rev 1990;43:67–97.
[15] Reddy JN, Robbins DH. Theories and computational models for composite laminates. Appl Mech Rev 1994;47:147–69.
[16] Carrera E. Developments, ideas and evaluations based upon Reissner's mixed variational theorem in the modeling of multilayered plates and shells. Appl Mech Rev 2001;54:301–29.
[17] Carrera E. Theories and finite elements for multilayered, anisotropic, composite plates and shells. Arch Comp Meth Eng 2002;9:1–60.
[18] Qatu MS, Sullivan RW, Wang W. Recent research advances on the dynamic analysis of composite shells: 2000–2009. Compos Struct 2010;93:14–31.
[19] Kulikov GM, Plotnikova SV. Solution of statics problems for a three-dimensional elastic shell. Doklady Phys 2011;56:448–51.
[20] Kulikov GM, Plotnikova SV. On the use of a new concept of sampling surfaces in shell theory. Adv Struct Mater 2011;15:715–26.
[21] Kulikov GM, Plotnikova SV. A method of solving three-dimensional problems of elasticity for laminated composite plates. Mech Comp Mater 2012;48:23–36.
[22] Kulikov GM, Plotnikova SV. Finite rotation geometrically exact four-node solid-shell element with seven displacement degrees of freedom. Comp Model Eng Sci 2008;28:15–38.
[23] Kulikov GM, Carrera E. Finite deformation higher-order shell models and rigid-body motions. Int J Solids Struct 2008;45:3153–72.
[24] Runge C. Über empirische Funktionen und die Interpolation zwischen äquidistanten Ordinaten. Z Math Physik 1901;46:224–43.
[25] Burden RL, Faires JD. Numerical analysis. Ninth ed. Boston: Brooks/Cole, Cengage Learning; 2010.
[26] Vlasov BF. On the bending of rectangular thick plate. Trans Moscow State Univ 1957;2:25–31.
[27] Pagano NJ. Exact solutions for rectangular bidirectional composites and sandwich plates. J Compos Mater 1970;4:20–34.
[28] Srinivas S, Rao AK. Bending, vibration and buckling of simply supported thick orthotropic rectangular plates and laminates. Int J Solids Struct 1970;6:1463–81.
[29] Srinivas S, Rao AK. A three-dimensional solution for plates and laminates. J Franklin Inst 1971;291:469–81.
[30] Pagano NJ, Hatfield SJ. Elastic behavior of multilayered bidirectional composites. AIAA J 1972;10:931–3.
[31] Pagano NJ. Influence of shear coupling in cylindrical bending of anisotropic laminates. J Compos Mater 1970;4:330–43.
[32] Noor AK, Burton WS. Three-dimensional solutions for antisymmetrically laminated anisotropic plates. J Appl Mech 1990;57:182–8.
[33] Savoia M, Reddy JN. A variational approach to three-dimensional elasticity solutions of laminated composite plates. J Appl Mech 1992;59:S166–75.